Title

The cross-over to magnetostrophic convection in planetary dynamo systems.

Journal

Proceedings. Mathematical, physical, and engineering sciences, 473(2199)

ISSN

1364-5021

Authors

Aurnou, JM
King, EM

Publication Date

2017-03-01

DOI

10.1098/rspa.2016.0731

Peer reviewed

PROCEEDINGS A

rspa.royalsocietypublishing.org

Perspective

Cite this article: Aurnou JM, King EM. 2017 The cross-over to magnetostrophic convection in planetary dynamo systems. *Proc. R. Soc. A* **473**: 20160731.
http://dx.doi.org/10.1098/rspa.2016.0731

Received: 26 September 2016
Accepted: 14 February 2017

Subject Areas:
Geophysics, Fluid mechanics, Astrophysics

Keywords:
magnetostrophic balance, dynamos, rotating convection, scaling theory

Author for correspondence:
J. M. Aurnou
e-mail: aurnou@ucla.edu

A contribution to the special feature 'Perspectives in astrophysical and geophysical fluids'.

The cross-over to magnetostrophic convection in planetary dynamo systems

J. M. Aurnou[1] and E. M. King[2]

[1]Earth, Planetary and Space Sciences, University of California, Los Angeles, CA 90095-1567, USA
[2]First Principles Research Group, Inc., Portland, OR 97210, USA

JMA, 0000-0002-8642-2962

Global scale magnetostrophic balance, in which Lorentz and Coriolis forces comprise the leading-order force balance, has long been thought to describe the natural state of planetary dynamo systems. This argument arises from consideration of the linear theory of rotating magnetoconvection. Here we test this long-held tenet by directly comparing linear predictions against dynamo modelling results. This comparison shows that dynamo modelling results are not typically in the global magnetostrophic state predicted by linear theory. Then, in order to estimate at what scale (if any) magnetostrophic balance will arise in nonlinear dynamo systems, we carry out a simple scaling analysis of the Elsasser number Λ, yielding an improved estimate of the ratio of Lorentz and Coriolis forces. From this, we deduce that there is a magnetostrophic cross-over length scale, $\mathcal{L}_X \approx (\Lambda_o^2/Rm_o)D$, where Λ_o is the linear (or traditional) Elsasser number, Rm_o is the system scale magnetic Reynolds number and D is the length scale of the system. On scales well above $\mathcal{L}_X$, magnetostrophic convection dynamics should not be possible. Only on scales smaller than $\mathcal{L}_X$ should it be possible for the convective behaviours to follow the predictions for the magnetostrophic branch of convection. Because $\mathcal{L}_X$ is significantly smaller than the system scale in most dynamo models, their large-scale flows should be quasi-geostrophic, as is confirmed in many dynamo simulations. Estimating $\Lambda_o \simeq 1$ and $Rm_o \simeq 10^3$ in Earth's core, the cross-over scale is approximately 1/1000 that of the system scale, suggesting that magnetostrophic convection dynamics exists in the core only on small scales below those that can be characterized by geomagnetic observations.

THE ROYAL SOCIETY PUBLISHING

1. Introduction

Earth's global magnetic field is continually regenerated via the fluid mechanical dynamo processes that operate in the liquid metal outer core (figure 1). The observable geomagnetic field predominantly emanates outwards from the core–mantle boundary (CMB) in the Southern Hemisphere, returning in the Northern Hemisphere such that the field is dominated by its axial dipole component. However, the CMB field is strongly crenallated with localized patches of magnetic flux existing over the full range of observable length scales [2]. The field also varies temporally over a broad range of scales, from mantle convection time scales [3] down to subdecadal periods [4,5].

One of the fundamental issues in planetary dynamo studies concerns the dynamical force balance that controls the style of core fluid dynamics that generates dynamo action. It has long been assumed that the dynamics state is in 'magnetostrophic balance', in which Lorentz, Coriolis and pressure forces dominate the system. This assumption stems from the linear analysis of Chandrasekhar [6], which showed that convection is greatly facilitated in the magnetostrophic regime. This has led workers to argue that the most efficient state of dynamo action must arise under magnetostrophic conditions. However, there is little evidence for leading order magnetostrophic balance in present-day dynamo simulations. To address this issue, we present scaling arguments here that suggest that magnetostrophic convection dynamics will develop only below a certain 'cross-over scale', and quasi-geostrophic dynamics will dominate at all larger scales.

The source of the fluid motions that drive the core dynamo is likely to be thermocompositional convection ([7,8], cf. [9]). It is presently unclear as to which buoyancy source, thermal or compositional, is the dominant convective driver [10,11]. This depends on the thermal conductivity of the core fluid [12,13], which determines how efficiently heat is conducted across the core and how much of this heat is available over to drive thermal convection in the fluid [14].

Irrespective of the buoyancy source, magnetic induction must be greater than magnetic diffusion in order for a dynamo to operate. The non-dimensionalized magnetic induction equation, which describes the growth or decay of magnetic fields in time, depends upon the parameter called the magnetic Reynolds number, Rm, which describes the balance between magnetic field generation and magnetic diffusion:

$$Rm = \frac{\boldsymbol{B}\cdot\nabla\boldsymbol{u}}{\eta\nabla^2\boldsymbol{B}} \sim \frac{U\mathcal{L}_B^2}{\eta\mathcal{L}_U}. \tag{1.1}$$

Here, $\boldsymbol{B}$ is magnetic induction, $\boldsymbol{u}$ is velocity measured in the body frame rotating with constant angular velocity $\boldsymbol{\Omega}$ and $\eta = 1/(\mu_o\sigma)$ is the fluid's magnetic diffusivity that varies inversely to the magnetic permeability μ_o and the fluid's electrical conductivity σ. The characteristic velocity scale is U. The respective scales of magnetic and velocity field structures are $\mathcal{L}_B$ and $\mathcal{L}_U$, and it is assumed here that the gradient scales are well approximated by the diameters of the relevant structures (i.e. $\nabla\boldsymbol{u} \sim U/\mathcal{L}_U$). The standard form of the magnetic Reynolds, Rm_o, is defined using only the system scale $D \sim \mathcal{L}_B \sim \mathcal{L}_U$:

$$Rm_o = \frac{U_o D}{\eta}, \tag{1.2}$$

where D is taken to be the radial thickness of the fluid shell in spherical dynamos and U_o is the large- or system-scale estimate of the core flow velocity (e.g. figure 11 in [5]). This system-scale magnetic Reynolds must have a value greater than $O(10)$ for sustained global-scale dynamo action to occur [15]. Observations of Earth's magnetic field produce estimates of $Rm_o \sim 10^3$ for the geodynamo [16].

By characterizing the non-dimensional length of a given structure as

$$\ell = \frac{\mathcal{L}}{D}, \tag{1.3}$$

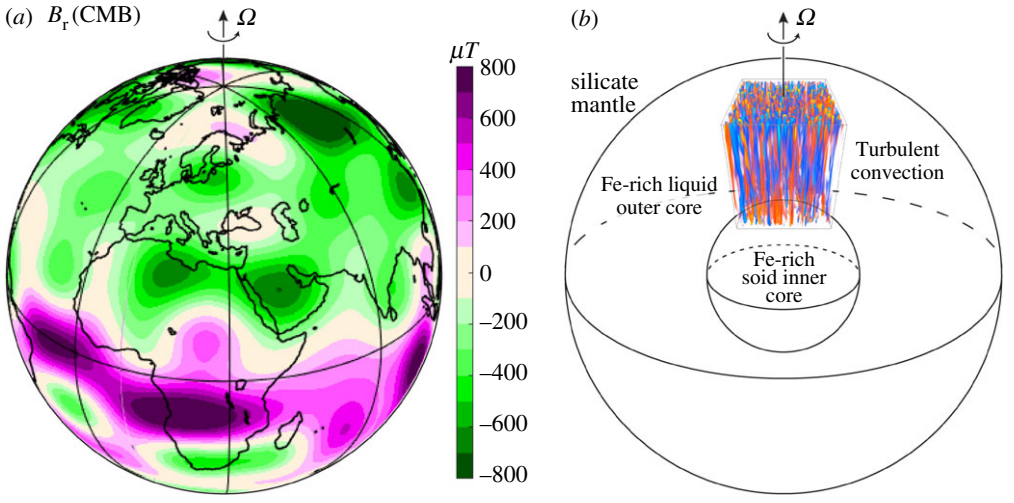

Figure 1. (*a*) Radial magnetic field on Earth's core–mantle boundary (CMB) viewed from near 20 degrees north latitude and 30 degrees east longitude. (Image: K. Soderlund.) (*b*) Schematized view of Earth's deep interior structure with colour rendering of hypothetical convection field in the fluid outer core. (Rendering: Julien *et al.* [1].)

the magnetic Reynolds number can then be recast as $Rm = Rm_o \ell_B^2/\ell_U$, where $\ell_B = \mathcal{L}_B/D$, $\ell_U = \mathcal{L}_U/D$. (In dynamo models, U_o and B_o are likely to be volumic root-mean-square (r.m.s.) values of U and B.) Equation (1.1) reduces to

$$Rm = Rm_o \ell \tag{1.4}$$

when considering the generalized length scale magnitude ℓ.

In addition to a sufficiently large Rm_o value, it has long been argued that Earth-like planetary dynamo action requires a global-scale, leading-order force balance between the Lorentz force F_L and the Coriolis force F_C, with the pressure force F_P primarily making up the difference [17,18]. This defines so-called *magnetostrophic balance* in the fluid:

$$0 = (\boldsymbol{F}_L + \boldsymbol{F}_C) + \boldsymbol{F}_P = (\boldsymbol{J} \times \boldsymbol{B} + 2\rho \boldsymbol{u} \times \boldsymbol{\Omega}) - \nabla p, \tag{1.5}$$

where $\boldsymbol{J}$ is the electric current density, ρ is fluid density and p is the pressure in the fluid. The buoyancy force must also exist to drive the convective flow $\boldsymbol{u}$. Taking note of this here, we will not consider this term in our considerations of magnetostrophic balance.

Magnetostrophic balance is typically estimated via the Elsasser number Λ, the ratio of Lorentz and Coriolis forces in the fluid:

$$\Lambda = \frac{\text{Lorentz}}{\text{Coriolis}} = \frac{\boldsymbol{J} \times \boldsymbol{B}}{2\rho \boldsymbol{\Omega} \times \boldsymbol{u}} \sim \frac{JB}{2\rho \Omega U}. \tag{1.6}$$

Using the $Rm \ll 1$ form of Ohm's law that neglects time variations in B, the current density scales as $J \sim \sigma U_o B_o$ [19,20]. This yields the traditional definition of the Elsasser number:

$$\Lambda_o = \frac{\sigma B_o^2}{2\rho \Omega}, \tag{1.7}$$

which is referred to here as the *linear Elsasser number*. The low Rm form of J employed in (1.7) does not accurately describe the large-scale magnetohydrodynamics (MHD) in dynamo systems where Rm_o must significantly exceed unity for global-scale dynamo action to be possible. Making use of $J \sim \sigma U_o B_o$ requires that the dynamics are occurring on a relatively small scale, $\ell < D$, such that $Rm \ll 1$ and thus conflates large- and small-scale MHD processes. In addition, because Λ_o is independent of length scale, it is natural (although incorrect) to posit that $\Lambda_o \sim 1$ dynamo systems

must be in magnetostrophic balance at all scales. This is a misinterpretation of the physical meaning of Λ_o, which is meaningful only on the small length scales at which $Rm \ll 1$.

We contend here that global-scale magnetostrophic balance does not occur in the vast majority of planetary dynamo models. Instead, the flows in these simulations are nearly all in a *quasi-geostrophic balance* in which Coriolis and pressure forces comprise the dominant force balance on large scales in the fluid [20–28]. This contention raises the following questions: under what conditions, if any, do the magnetostrophic predictions of linear theory apply to nonlinear planetary dynamo systems? Does magnetostrophic balance manifest at any length scale of planetary core convection? And if so, do our planetary dynamo models get this right?

In an attempt to address these questions, the results of the plane-layer linear theory of rotating magnetoconvection [6] are compared with the results of recent planetary dynamo models carried out in spherical shell geometries. It can be argued that these two systems, disparate in terms of geometry and Rm_o values, cannot be meaningfully related (cf. [29]). However, this intercomparison is ubiquitously made in the dynamo literature when considerations of magnetostrophic balance are put forth. We intend to define when such comparisons are justified.

To do so, the predictions of linear rotating magnetoconvection theory are presented in §2 and are then directly compared with the results of current numerical planetary dynamo experiments in §3. This makes clear that there is little evidence for global-scale magnetostrophic balance in typical planetary dynamo models. In §4, we reconsider the formulation of the Elsasser number, extending the work of [20,23] and providing a new magnetostrophic 'cross-over scale' $\ell_\chi \simeq \Lambda_o^2/Rm_o$. We argue that magnetostrophic balance can manifest only on flow scales below ℓ_χ, and that quasi-geostrophic convection dynamics will dominate on all scales greater than ℓ_χ. Finally, in §5, we discuss the implications and limitations of ℓ_χ and how it can be used to interpret planetary dynamo modelling results and observations.

2. A foray into linear theory

The concept that planetary dynamos evolve to a global magnetostrophic state was first posited following Chandrasekhar's linear stability analysis of plane layer rotating magnetoconvection [6,30]. The linear theory predicts that convection develops from the stationary $\boldsymbol{u} = 0$ ($Rm = 0$) state most easily in the presence of an $\Lambda_o \simeq 1$ imposed magnetic field [6,31]. Thus, the interaction of strong magnetic forces and comparably strong rotational forces allows the onset of convection to occur more easily. In contrast, convective onset would be strongly suppressed were either of these forces to act alone [32]. This has led to the idea that convection-driven dynamos will naturally function most efficiently in the magnetostrophic regime where the convection itself is most efficient (e.g. [33,34], cf. [35]).

Chandrasekhar famously derived the dispersion relations for convection in a plane layer of electrically conducting fluid with vertically oriented rotation and magnetic field vectors [6]. Qualitatively similar results are found in the case of a horizontally imposed magnetic field, although linear magnetostrophic effects are predicted to arise at somewhat lower values of Λ_o [36,37]. Further, spherical analyses of linear rotating magnetoconvection produce qualitatively similar asymptotic scalings [38], albeit with an array of additional complexities [39].

For isothermal, mechanically stress-free, electrically insulating boundary conditions, the dispersion relation for steady convection in a fluid of vertical layer depth D is given by equation (4.59) in Chandrasekhar's treatise [6], and the equations necessary to solve for oscillatory convection are given by equations (4.65) and (4.66). Onset solutions that are 'steady' vary in space, but are stationary and do not vary in time. In contrast, in cases of 'oscillatory' onset, the motions that first develop oscillate sinusoidally in time.

Solutions of these dispersion relations are presented here in terms of the following parameters (for detailed definitions, see [40]). The Rayleigh number,

$$Ra = \frac{\alpha g \Delta T D^3}{\nu \kappa},$$

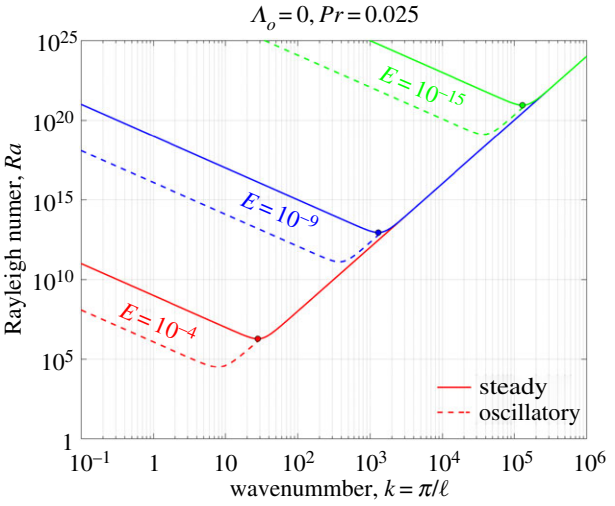

Figure 2. Non-magnetic rotating convection ($\Lambda_o = 0$) marginal stability curves (Ra-k) in a liquid metal ($Pr = 0.025$). The solid (dashed) lines denote steady (oscillatory) convective onset conditions. Red, blue and green lines show the $E = 10^{-4}$, $E = 10^{-9}$ and $E = 10^{-15}$ stability curves, respectively. The coloured circles mark the minima of the steady marginal stability curves and, thus, demarcate the values of the critical Rayleigh number Ra_{crit} and critical wavenumber k_{crit} values at a given E value at which the onset of steady convection occurs. Identical coloured circles carry the same information in figures 3, 6 and 8.

describes the non-dimensional buoyancy forcing, where α is thermal expansivity, g is gravitational acceleration, ΔT is the superadiabatic temperature difference across the fluid layer, ν is the kinematic viscosity and κ is thermal diffusivity. The Ekman number,

$$E = \frac{\nu}{2\Omega D^2},$$

is the ratio of the viscous and Coriolis forces. The Prandtl number,

$$Pr = \frac{\nu}{\kappa},$$

is the ratio of the thermal and viscous diffusion time scales, whereas the magnetic Prandtl number,

$$Pm = \frac{\nu}{\eta},$$

is the ratio of the magnetic and viscous diffusion times. In the linear theory, the magnetic field is not self-generated, as occurs in a dynamo. The strength of the imposed field is typically denoted in linear studies of rotating magnetoconvection by the value of Λ_o [18,33,41–43]. Chandrasekhar [6,30], however, denotes the strength of the imposed magnetic field via what is now called the Chandrasekhar number, $Q = \Lambda_o/E$, which estimates the ratio of the Lorentz and viscous forces (in the low Rm limit). Lastly, spatial scales are often discussed in theoretical analyses in terms of the wavenumber, $k = \pi/\ell$, where $\ell = \mathcal{L}/D$ is taken to be half of a wavelength.

Figure 2 shows Ra-k marginal stability curves for non-magnetic ($\Lambda_o = 0$) rotating convection in a core-like liquid metal with $Pr = 0.025$ [44]. The red, blue and green curves denote solutions at $E = 10^{-4}$, 10^{-9} and 10^{-15}, respectively. The solid curves mark the marginal values for steady convection, which denote the lowest Ra value at which convection will develop for a given value of k. The dashed curves demarcate the marginal Ra-k values for the oscillatory mode of convection, which only develop in fluids for which $Pr < 0.67$ [6,45]. Each of these marginal stability curves has a simple 'U'-shape, with a single global minimum value of Ra as a function of k. This global minimum in each curve denotes the critical Rayleigh number, Ra_{crit}, and the corresponding k_{crit} value sets the critical length scale ℓ_{crit} at which the onset of convection will occur at a given value of the Ekman number E. The small, coloured circles demarcate Ra_{crit}-k_{crit} for each of the three steady marginal stability curves.

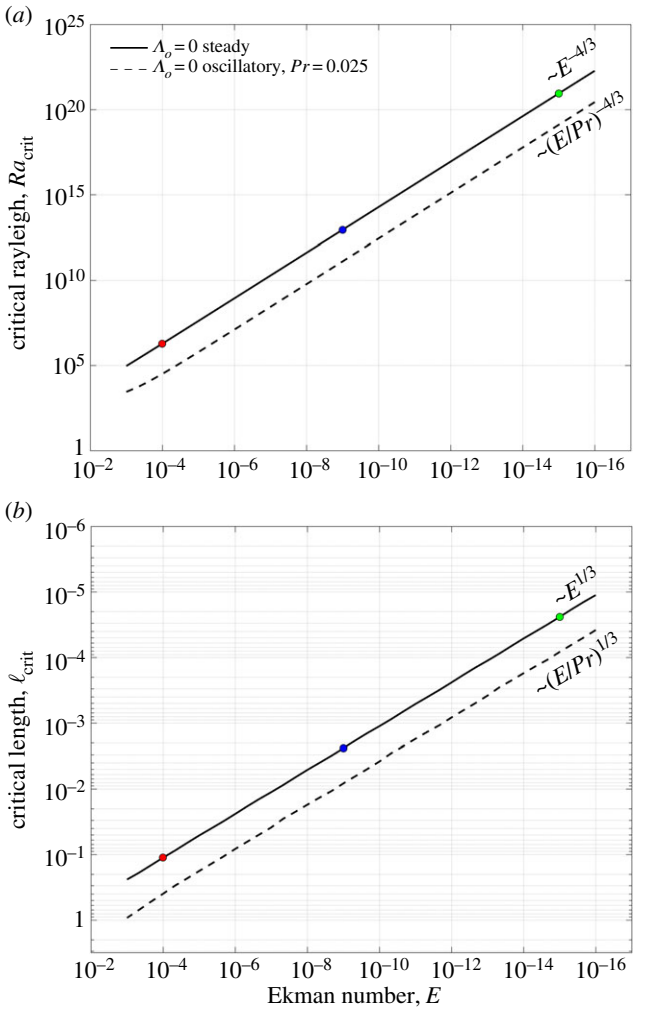

Figure 3. Linear rotating convection ($\Lambda_o = 0$) predictions for liquid metal ($Pr = 0.025$): (*a*) critical Rayleigh number, Ra_{crit}; (*b*) critical length scale, $\ell_{crit} = \pi/k_{crit}$. The solid black lines demarcate the onset values for steady convection, which has no dependence on the Prandtl number Pr. The dashed black lines denote the onset of oscillatory convective motions, which can occur only for $Pr < 0.67$ [6]. The coloured circles correspond to those shown in figure 2.

Figure 3*a*,*b*, respectively, shows curves of Ra_{crit} and $\ell_{crit} = \pi/k_{crit}$ as a function of Ekman number for $Pr = 0.025$ plane layer rotating convection ($\Lambda_o = 0$). The Ekman number values range from the highest values used in planetary dynamo models ($E = 10^{-3}$) down to low values relevant to Earth's core ($E = 10^{-16}$). These E values are plotted with the smallest values to the right, in hopes of making clear that very low E values correspond to the extremely rapidly rotating conditions that exist in planetary cores [46]. The three-coloured circles in each panel allow one to connect the results for the three E curves in figure 2 to the results shown in figure 3*a*,*b*.

The curves shown in figure 3 agree well with the $E \to 0$ asymptotic scalings of [45]. The $E \to 0$ onset predictions for steady rotating convection yield

$$Ra_{crit} = 8.7E^{-4/3} \quad \text{and} \quad \ell_{crit} = 2.4E^{1/3}, \tag{2.1}$$

whereas the predictions for oscillatory rotating convection in $Pr < 0.67$ fluids are

$$Ra_{crit} = 17.4\left(\frac{E}{Pr}\right)^{-4/3} \quad \text{and} \quad \ell_{crit} = 2.4\left(\frac{E}{Pr}\right)^{1/3}. \tag{2.2}$$

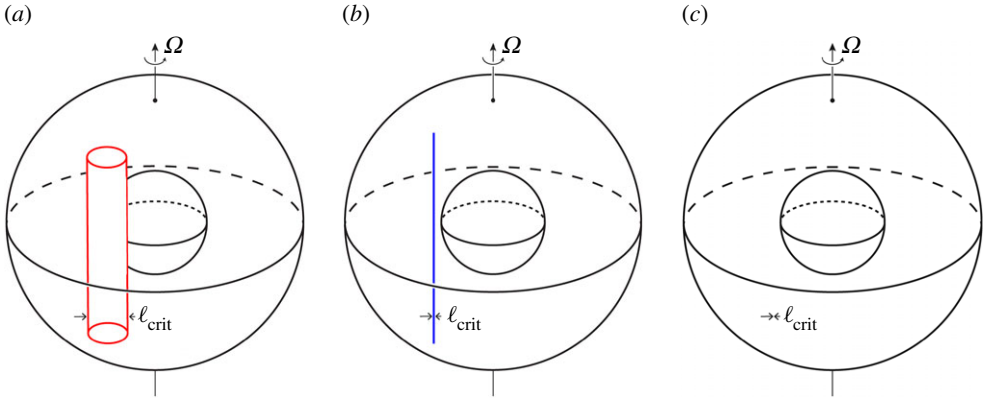

Figure 4. Schematic shows the properly scaled linear onset scale ℓ_{crit} for steady convection for the three Ekman values shown in figure 2: (*a*) $E = 10^{-4}$; (*b*) $E = 10^{-9}$; (*c*) $E = 10^{-15}$. In panel (*c*), the $E^{1/3}$ onset scale is close to 10^{-5} the width of the fluid shell *D*. Plotted using vector graphics, this convection structure does not appear visible in the image.

Using $Pr = 0.025$, as in figure 3, we estimate that the onset of oscillatory convection (dashed line) will occur at a critical Rayleigh number that is approximately $(17.4/8.7)\, Pr^{4/3} \approx 1.5\%$ that of the critical *Ra* value for steady convection (solid lines) at a given *E* value. Further, the oscillatory onset scale in a $Pr = 0.025$ fluid is predicted to be larger than the steady onset scale by a factor near to $Pr^{-1/3} \approx 3$ [47].

Figure 3*b* predicts an extreme range of ℓ_{crit} values over the range of *E* values considered. These ℓ_{crit} values are plotted with the smallest values towards the top of the figure, in hopes of making clear that very small-scale convective flows are predicted for low *E* conditions that exist in planetary cores. The scales of such structures are shown schematically in figure 4 within Earth-like spherical shell geometries. Quasi-geostrophic, axially aligned convection columns dominate the flow field [48,49]. In typical present-day dynamo models, carried out at $E \simeq 10^{-4}$, these columnar structures are large, with $\ell_{crit} \sim 10^{-1}$. At $E = 10^{-9}$, the 'grand challenge' value proposed in [50], rotating convection structures will develop with roughly one thousand structures circumscribing the outer core fluid volume ($\ell \sim 10^{-3}$). Finally, at the core value of $E = 10^{-15}$, approximately 10^5 rotating convection onset structures are predicted to circumscribe the core ($\ell \sim 10^{-5}$). Such high wavenumber hydrodynamic structures are so small in scale that they are subpixel in figure 4*c*, and, thus, are not visible. Similarly, such structures are approximately four orders of magnitude below the limits of planetary magnetic field observations. Thus, individual $\Lambda_o = 0$ onset-scale convection columns, should they exist in Earth's core, are then not relevant to our interpretation of geomagnetic flux patches or their temporal variations [24,51,52].

When a dynamically strong magnetic field is added, drastic changes, both qualitative and quantitative, occur in the nature of the marginal stability curves. Figure 5 shows *Ra*-*k* marginal stability curves for $\Lambda_o = 1$ rotating magnetoconvection cases in a core-like liquid metal with $Pr = 0.025$ and $Pm = 10^{-6}$ [44]. As in figure 2, the red, blue and green curves denote solutions at $E = 10^{-4}$, 10^{-9} and 10^{-15}, respectively. The solid curves mark the marginal values for steady convection, and the dashed curves demarcate the marginal *Ra*-*k* values for oscillatory convective modes [6]. For $\Lambda_o \sim 1$ rotating magnetoconvection, the marginal stability curves no longer have simple 'U'-shaped wells, like those found for the rotating convection curves in figure 2. Instead, there is a broad well on the left side of this plot centred near $k \simeq 3$, which corresponds to the steady magnetostrophic convection branch. At higher wavenumbers, the geostrophic convective modes dominate, such that the marginal stability curves are similar to the rotating convection curves of figure 2. Except at $E = 10^{-4}$ (where the wells are nearly overlapping), the critical Rayleigh number Ra_{crit} is determined by the low wavenumber (e.g. $k_{crit} \simeq 3$; $\ell_{crit} \simeq 1$) minimum of the steady magnetostrophic convection branch.

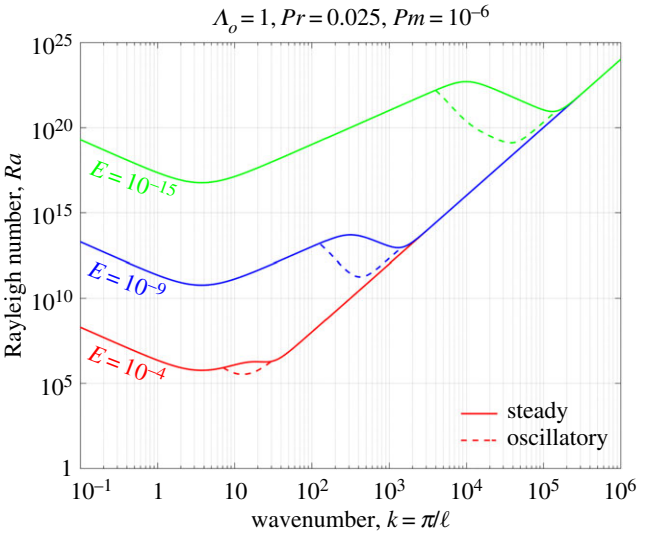

Figure 5. Rotating magnetoconvection ($\Lambda_o = 1$) marginal stability curves (Ra-k) in a liquid metal ($Pr = 0.025$, $Pm = 10^{-6}$). The solid (dashed) lines denote steady (oscillatory) convective onset conditions. Red, blue and green lines, respectively, show the stability curves at $E = 10^{-4}$, $E = 10^{-9}$ and $E = 10^{-15}$.

Figure 6 shows the $\Lambda_o = 1$, $Pr = 0.025$, $Pm = 10^{-6}$ linear rotating magnetoconvection $Ra_{\rm crit}$ and $\ell_{\rm crit} = \pi/k_{\rm crit}$ predictions (blue lines) as a function of Ekman number. These $\Lambda_o = 1$ onset values are overlain atop the $\Lambda_o = 0$ rotating convection results (black lines) from figure 3. The critical values for oscillatory rotating convection (dashed blue line) asymptote to the same solutions as the oscillatory rotating convection branch (dashed black line), as may be inferred by comparing figures 2 and 5. The presence of the imposed magnetic field acts only to alter the oscillation frequencies of the oscillatory $\Lambda_o = 1$ convection branch. These frequencies (which are not shown) are significantly decreased relative to the faster inertial frequencies found in $\Lambda_o = 0$ rotating convection solutions [6,45].

In contrast to the oscillatory branch, the steady rotating magnetoconvection branch is fundamentally different from the rotating convection solutions. The solid blue line shows that the onset of the steady rotating magnetoconvection solution varies as $Ra_{\rm crit} \sim E^{-1}$ and has the lowest possible critical Rayleigh value for $E \lesssim 10^{-8}$. Thus, steady linear rotating magnetoconvection should develop at Ra values $\sim E^{1/3}$ lower than steady rotating convection and $\sim (E/Pr^4)^{1/3}$ lower than oscillatory rotating convection. This suggests that steady rotating magnetoconvection will develop at significantly lower Ra values than can occur in rotating convection. For example, using $E = 10^{-15}$ and $Pr = 0.025$, the linear theory predicts $Ra_{\rm crit} = 5.75 \times 10^{16}$ for steady rotating magnetoconvection, which is 6.6×10^{-5} the predicted critical value for steady rotating convection and 4.5×10^{-3} that for oscillatory rotating convection.

The length scale information given in figure 6*b* shows that steady rotating magnetoconvection develops at $\ell_{\rm crit} \sim O(1)$. Thus, the linear analysis predicts a factor of $\sim E^{-1/3}$ increase in flow scale for $\Lambda_o \approx 1$ relative to $\Lambda_o = 0$ rotating convection cases at the same E. This massive change in scale—effectively from the micro-scale at $\Lambda_o = 0$ (figure 4*c*) to global scale at $\Lambda_o = 1$—should be easily detected in dynamo systems in global magnetostrophic balance. We propose, following [20], to use this fundamental change in scale between geostrophically balanced rotating convection and magnetostrophically balanced rotating magnetoconvection to infer the presence of the magnetostrophic branch of convection. Thus, we will focus on this large alteration in convective flow scale in comparing dynamo model results against linear theory in the following section.

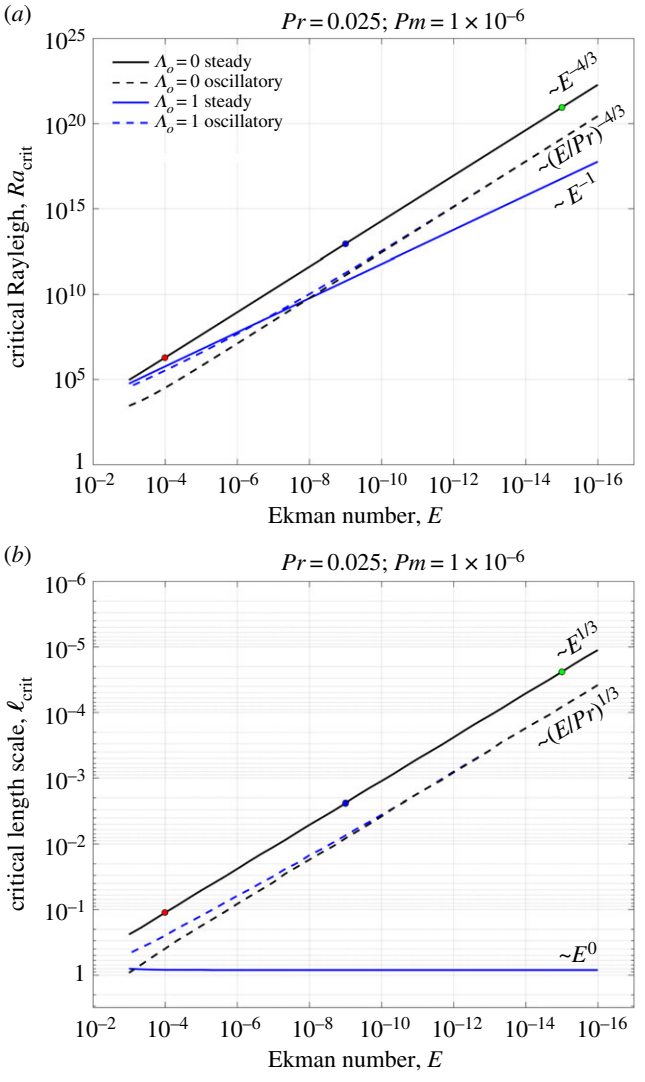

Figure 6. Linear rotating convection ($\Lambda_o = 0$, black lines) and rotating magnetoconvection ($\Lambda_o = 1$, blue lines) predictions for liquid metal ($Pr = 0.025$): (*a*) critical Rayleigh number, Ra_{crit}; (*b*) critical length scale, $\ell_{crit} = \pi/k_{crit}$. The solid (dashed) lines demarcate the linear predictions for steady (oscillatory) convection. The coloured circles correspond to the three circles in figure 2.

3. Comparing spherical dynamo models against planar theory

We have assembled the results from a small subset of planetary dynamo modelling studies [20, 53–56] for comparison with the linear theoretical predictions. These dynamo modelling results are summarized in table 1, with typical estimates for Earth given in the top row. Our sampling of recent models is in no way comprehensive (cf. [57,58]), but the results are all relatively recent and cover a broad range of input parameter values, e.g. $10^{-3} \geq E > 10^{-8}$, as well as output parameter values, e.g. $0.06 < \Lambda_o < 6$.

Linear theory predicts that increasing the value of Λ_o at fixed E can induce a sharp transition from the small-scale $\ell_{crit} \sim E^{1/3}$ rotating convection branch (also called the geostrophic branch) to the large-scale $\ell_{crit} \sim O(1)$ magnetoconvection branch (also called the magnetostrophic branch) [6,18,42,59]. Steady, linear magnetostrophic convection is predicted to arise for $\Lambda_o \geq 4.5E^{1/3}$ [18]. Figure 7 shows E plotted versus Λ_o from the data in table 1. All the dynamo cases in table 1 are

Table 1. Geodynamo estimates ($Pr \sim 10^{-2}$ to 10^{3}) and $Pr = 1$ dynamo model results for comparison with linear rotating magnetoconvection theoretical predictions. These selected results are from Sreenivasan [53], Soderlund *et al.* [20,54], Sheyko [55] and Schaeffer *et al.* [56]. Since the flux Rayleigh number $Ra_F = NuRa$ is the thermal forcing parameter in Schaeffer *et al.* [56], we estimate their Ra values as Ra_F/Nu, where Nu denotes the Nusselt number values reported in their study.

	E	Ra	Pm	Λ_o	Rm_o	ℓ_χ	$\ell_{B_\mathcal{E}}$	$\ell_{U_\mathcal{E}}$	ℓ_{B_∇}	ℓ_{U_∇}
Earth	1.0×10^{-15}	—	$\simeq 1 \times 10^{-6}$	$\simeq 1000$	$\simeq 1 \times 10^{-3}$	—	—	—	—	—
[53]	5.0×10^{-5}	4.88×10^{6}	1	$\simeq 1$	—	—	—	1.8×10^{-1}	—	—
	1.5×10^{-6}	2.17×10^{9}	0.1	$\simeq 1$	—	—	—	5.4×10^{-2}	—	—
[20]	1.0×10^{-3}	6.50×10^{4}	5	4.34	50	3.8×10^{-1}	4.0×10^{-1}	4.4×10^{-1}	—	—
[54]	1.0×10^{-4}	1.42×10^{6}	2	1.30	68	2.5×10^{-2}	2.7×10^{-1}	2.1×10^{-1}	—	—
	1.0×10^{-5}	3.10×10^{7}	2	4.84	156	1.5×10^{-1}	2.1×10^{-1}	1.4×10^{-1}	—	—
[55]	1.18×10^{-6}	1.86×10^{8}	0.2	0.07	63	7.7×10^{-5}	4.2×10^{-1}	6.9×10^{-2}	—	—
	2.96×10^{-7}	2.22×10^{10}	0.05	3.61	274	4.8×10^{-2}	2.0×10^{-1}	5.5×10^{-2}	—	—
[56]	5.0×10^{-6}	2.05×10^{8}	0.4	5.77	709	4.7×10^{-2}	—	—	4.0×10^{-2}	4.0×10^{-2}
	5.0×10^{-7}	2.82×10^{9}	0.2	5.66	662	4.8×10^{-2}	—	6.7×10^{-2}	4.4×10^{-2}	2.1×10^{-2}
	5.0×10^{-8}	4.31×10^{10}	0.1	1.81	587	5.6×10^{-3}	—	2.9×10^{02}	3.4×10^{-2}	1.1×10^{-2}

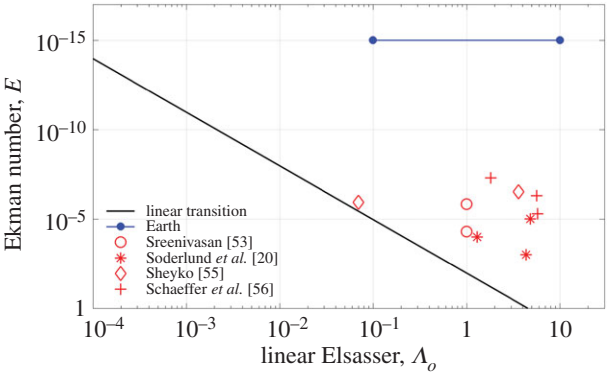

Figure 7. Linear predictions of the transition to plane layer magnetostrophic convection in the presence of a vertical imposed magnetic field, marked by the solid black line $\Lambda_o E^{-1/3} \simeq 4.5$ (e.g. see (64d) in [18]). The dynamo models in table 1 are all over the line, showing that linear theory predicts that these models should operate in the magnetostrophic convection regime. However, this prediction is not born out: the length scale information in figure 8*b* does not follow the $\ell \sim O(1)$ linear magnetostrophic scaling branch.

predicted to lie in the linear magnetostrophic convection regime. Thus, the expectation, based on plane layer theory, is that the characteristic scale of flow in these dynamo models will roughly follow the magnetostrophic trend $\ell \sim O(1)$ and should track approximately along the solid blue curve in figure 6*b*.

In figure 8, in table 1, Rayleigh numbers and characteristic flow scales are plotted as a function of Ekman number. The linear theoretical predictions are shown for comparison. Only steady convection solutions (solid lines) are displayed since $Pr > 0.67$ in all the table 1 dynamo models. Figure 8*a* shows that the Ra values track reasonably well with the $E^{-4/3}$ trend of the geostrophic branch of convection. Even though the precise Ra_{crit} values differ from the plane layer linear theoretical predictions owing to the effects of spherical geometry [48,59–61], the plane layer predictions still provide an adequate qualitative proxy [20].

Figure 8*b* shows the typical flows scales in the table 1 dynamo cases plotted versus E. The red and black symbols show the characteristic kinetic energy weighted length scales computed as

$$\ell_{U_\mathcal{E}} = \frac{\pi}{\bar{k}_U}, \quad \text{where } \bar{k}_U = \sqrt{\frac{\sum k(\boldsymbol{u}_k \cdot \boldsymbol{u}_k)}{2\mathcal{E}_U}}, \tag{3.1}$$

where $\bar{k}_U$ is the kinetic energy weighted flow wavenumber and $\mathcal{E}_U$ is the volumic kinetic energy density (cf. [20,57]). The black asterisks show hydrodynamic ($Pm = 0$) solutions from [20], whereas the red asterisks show the corresponding dynamo solutions. The magenta plus-signs show the characteristic scales in [56] computed as the integral of the rms velocity divided by the rms vorticity of the bulk fluid,

$$\ell_{U_\nabla} = \frac{U_{\mathrm{rms}}}{\omega_{\mathrm{rms}}}. \tag{3.2}$$

We call ℓ_{U_∇} the 'gradient scale' of the flow, as it approximates the length scales at which the characteristic velocity gradients exist in a given flow field. (We employ analogous definitions exist for the magnetic energy-weighted scale of the magnetic field $\ell_{B_\mathcal{E}} = \pi/\bar{k}_B$ and the magnetic gradient scale $\ell_{B_\nabla} = B_{\mathrm{rms}}/J_{\mathrm{rms}}$ reported in table 1.)

The characteristic flow scales ℓ_U do not follow the magnetostrophic trend, irrespective of the length scale estimation method. Instead, the characteristic ℓ_U values track relatively closely to the small-scale $E^{1/3}$ geostrophic branch. It must be noted though that the energy-weighted estimates somewhat exceed the ℓ_{crit} predictions. One possibility is that the flows have increased to the

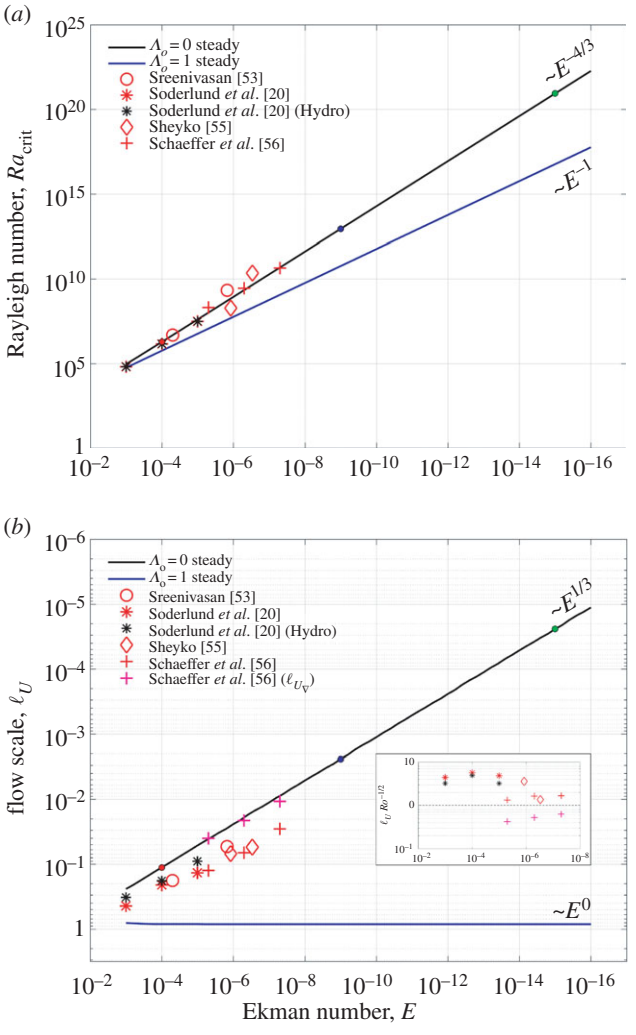

Figure 8. Results of $Pr = 1$ dynamo models from table 1 plotted atop the linear predictions for steady $\Lambda_o = 0$ and $\Lambda_o = 1$ convection. (*a*) dynamo *Ra* values (symbols) versus Ra_{crit} predictions (solid lines); (*b*) dynamo ℓ_U values (symbols) versus ℓ_{crit} predictions (solid lines). All the values shown are measurements of ℓ_{U_ϵ}, except the pink plus signs which show ℓ_{U_∇} values from [56]. Inset in (*b*): dynamo ℓ_U values normalized by the hydrodynamic turbulence scaling estimate $Ro^{1/2} = (Rm\,E/Pm)^{1/2}$. The dynamo length scales in (*b*) can be adequately described by either the non-magnetic $E^{1/3}$ onset scale or the $Ro^{1/2}$ turbulent scale, but not by the $\ell \sim O(1)$ linear magnetostrophic convection trend.

turbulent hydrodynamic length scale that grows in proportion to the square-root of the Rossby number, $Ro^{1/2} = \sqrt{Rm_o E/Pm}$ (e.g. see equation (12) in [53]). The inset panel in figure 8*b* shows the characteristic flow scales normalized by $Ro^{1/2}$. With $\ell_U/Ro^{1/2}$ values in the vicinity of unity, it is plausible that the flow scales are tracking either the geostrophic onset scale $\ell_U \sim E^{1/3}$ or the geostrophic turbulence scale $\ell_U \sim Ro^{1/2}$. It is difficult to disambiguate as to which hydrodynamic flow scaling is dominant over the range of E and Ro values presently accessible in planetary dynamo models [18,51,58,62]. The essential point here, though, is that the flow scales are not trending along the $\ell = O(1)$ magnetostrophic branch. This demonstrates that the table 1 nonlinear dynamo models are not in global magnetostrophic balance. Subsequently, our comparison of planetary dynamo results against plane layer linear theory shows that $\Lambda_o \sim 1$ dynamo values are not predictive of global scale magnetostrophic convection.

4. Crossing into the magnetostrophic convection regime

(a) Estimating the cross-over scale

In this section, we further develop the ideas of Soderlund *et al.* [20,23] in order to estimate the convective flow scales at which magnetostrophic balance should exist in high Rm_o dynamo settings.

Linear theory requires that motions are just beginning to be excited, such that $Rm \to 0$ for all scales ℓ. This differs fundamentally from the geodynamo, for instance, where $Rm_o \sim 10^3$. At high Rm values, one cannot use the low Rm scaling of Ohm's law, $J \sim \sigma UB$. Instead, Ampere's law (under the magnetohydrodynamic approximation) provides a more accurate estimate of the current density,

$$J = \frac{\nabla \times \boldsymbol{B}}{\mu_o} \sim \frac{B}{\mu_o \mathcal{L}_B}. \tag{4.1}$$

Substituting (4.1) in (1.6) yields the Elsasser number definition appropriate to $Rm_o > O(1)$ dynamo settings:

$$\Lambda \simeq \frac{B^2}{2\mu_o \rho \Omega U \mathcal{L}_B}. \tag{4.2}$$

Relationship (4.2) makes clear that the ratio of Lorentz and Coriolis forces is a scale-dependent quantity (as also shown in [20,23,63]). The value of the Elsasser number varies as $\mathcal{L}_B^{-1}$, so that the smaller the length scale of magnetic field variations, the greater the relative strength of the Lorentz forces.

Over the observable range of magnetic field scales, $1 \gtrsim \ell \gtrsim 0.1$, it has been postulated that Earth's magnetic and kinetic energy spectra remain flat on the CMB (e.g. figure 6 in [18]). Based on this, we will assume from here onwards that $\beta \simeq \alpha \simeq 0$ at the large observable scales. These assumptions allow (4.2) to be simplified to

$$\Lambda \simeq \frac{\Lambda_o}{Rm} = \left[\frac{\Lambda_o}{Rm_o}\right] \frac{1}{\ell_B}. \tag{4.3}$$

We contend that (4.3) gives a reasonable, heuristic estimate of Λ based on large-scale planetary observations. (In contrast, if one were analysing high-resolution dynamo modelling results, more accurate estimates of the scale variation in Λ would likely be found using (5.3) to better take into account the scale dependences of U and B.)

In order to estimate the flow scale at which magnetostrophic convection can arise ($\Lambda \approx 1$) using the simplified relationship (4.3), we must recast ℓ_B in terms of ℓ_U. This estimate is made by assuming quasi-steady induction:

$$B_o \frac{U_o}{\mathcal{L}_U} \sim \eta \frac{B_o}{\mathcal{L}_B^2}, \tag{4.4}$$

such that

$$\ell_B \sim \left(\frac{\ell_U}{Rm_o}\right)^{1/2}. \tag{4.5}$$

Note that the flow scale is taken to be $\mathcal{L}_U$ in the two expressions above, whereas the flow scale was taken to be D in Soderlund *et al.* [20].

Inserting (4.5) into (4.3) yields

$$\Lambda \sim \left(\left[\frac{\Lambda_o^2}{Rm_o}\right] \frac{1}{\ell_U}\right)^{1/2}. \tag{4.6}$$

The quantity in square brackets in (4.6) can be interpreted as a non-dimensional length scale. This characteristic length is called the *magnetostrophic cross-over scale*,

$$\ell_X = \frac{\Lambda_o^2}{Rm_o}, \quad \text{such that } \Lambda \sim \left(\frac{\ell_X}{\ell_U}\right)^{1/2}. \tag{4.7}$$

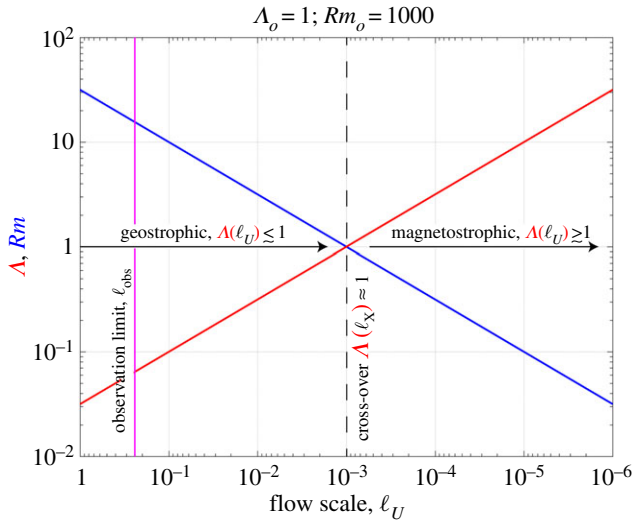

Figure 9. Heuristic scaling model shows the covariation of $\Lambda \simeq (\ell_X/\ell_U)^{1/2}$ (solid red line) and $Rm \simeq Rm_o \ell_B \sim (Rm_o \ell_U)^{1/2}$ (solid blue line) as a function of the flow scale ℓ_U. This model assumes that the characteristic velocity and magnetic field magnitude estimates, U_o and B_o, are scale invariant. Earth-like values of $\Lambda_o = 1$ and $Rm_o = 10^3$ generate an estimated value of the cross-over scale of $\ell_X = \mathcal{L}_X/D = 10^{-3}$ (dashed black line), below which magnetostrophic convection dynamics are predicted to develop in nonlinear $Rm_o \gg 1$ dynamo systems. The solid magenta line approximates the smallest observable scales of geomagnetic field variations ℓ_B. This limiting value is estimated as $\ell_{obs} \simeq \pi/n_{max}$, where $n_{max} = 13$ is the maximum resolved spherical harmonic degree in current geomagnetic field inversions [5].

The cross-over scale provides a simple physical interpretation of Λ in nonlinear dynamo systems: Lorentz forces are expected to be dynamically subdominant ($\Lambda < 1$) on flow scales ℓ_U well above the cross-over scale, whereas Lorentz forces may play a role in the dynamical balances ($\Lambda > 1$) on flow scales below ℓ_X. Because it is possible to estimate ℓ_X using remotely estimated values of B_o and $U_o(B_o)$ [5,64], the value of ℓ_X provides a zeroth-order estimate of the scale below which magnetostrophic convection may develop in a given dynamo system.

(b) A heuristic cross-over scale model

Figure 9 shows a hypothetical model for Rm (blue line) and Λ (red line) plotted versus non-dimensional flow scale ℓ_U in a system with Earth-like values of $\Lambda_o = 1$ and $Rm_o = 10^3$. As above, we assume scale invariant velocity and magnetic field estimates, $U \sim U_o$ and $B \sim B_o$. For $\ell_U \simeq 1$ system scale flows, relationship (4.5) yields $Rm = (Rm_o \ell_U)^{1/2} = Rm_o^{1/2}$ and $\Lambda = Rm_o^{-1} \ll 1$. Thus, the Lorentz forces are far weaker than the Coriolis forces on the largest length scales (as shown previously in [20,23]). With decreasing scale, Rm decreases in proportion to $\ell_U^{1/2}$ while Λ increases in proportion to $\ell_U^{-1/2}$.

At the magnetostrophic cross-over scale, the value of Λ reaches unity. On scales below ℓ_X, Λ exceeds unity and the dynamics should come into local magnetostrophic balance. Thus, in $Rm_o > O(1)$ dynamo systems, our simple model predicts that a magnetostrophic force balance can be established only on flow field scales $\ell_U \lesssim \ell_X$, whereas a primarily geostrophic balance of forces will hold for $\ell_U \gtrsim \ell_X$.

The magenta line in figure 9 approximates the smallest non-dimensional length scale, ℓ_{obs}, of the observable geomagnetic field structures on the CMB. This is estimated as $\ell_{obs} = \pi/n_{max}$, where $n_{max} = 13$ is the highest spherical harmonic degree resolved in present-day geomagnetic field models [2,5]. The corresponding dimensional scale is $\mathcal{L}_{obs} \sim 500$ km [2,18]. In contrast, the dimensional value of the cross-over scale in Earth's core is $\mathcal{L}_X = (\Lambda_o^2/Rm_o)D \simeq 2$ km, using $\Lambda_o \sim 1$,

$Rm_o \sim 10^3$ and $D \simeq 2260$ km as the depth of the outer core fluid depth. Our magnetostrophic cross-over scale estimates for flow structures in the core are far smaller than the smallest observable geomagnetic field scale. This implies that the observable part of Earth's magnetic field are best described by quasi-geostrophic dynamo processes [22,24,26], in agreement with recent interpretations of geomagnetic secular variation data [5,65].

(c) Cross-over Ekman number estimates

It may also be of interest to estimate if magnetostrophic conditions are expected to arise for a given dynamo system's input parameters. For instance, if we assume that the rotating convective onset scale is dominant, $\ell_U = E^{1/3}$ can be inserted into (4.6), giving

$$\Lambda \sim \left(\frac{\Lambda_o^2}{Rm_o} \frac{1}{E^{1/3}} \right)^{1/2}. \tag{4.8}$$

Assuming magnetostrophic conditions occur at $\Lambda \approx 1$, solving for E yields an estimate for the *cross-over Ekman number* value for $E^{1/3}$-scale flow:

$$E_{\mathrm{X,onset}} \sim \frac{\Lambda_o^6}{Rm_o^3} = \ell_{\mathrm{X}}^3. \tag{4.9}$$

If $E < E_{\mathrm{X,onset}}$, flows occurring on the $E^{1/3}$-scale will be affected by Lorentz forces. In contrast, if $E > E_{\mathrm{X,onset}}$, the onset scales are likely to be too large to feel significant magnetic effects. When the turbulent hydrodynamic scale, $\ell_U = Ro^{1/2} = (Rm_o E/Pm)^{1/2}$, is substituted into (4.6), the cross-over Ekman number then scales as

$$E_{\mathrm{X,turb}} \sim \frac{\Lambda_o^4\, Pm}{Rm_o^3}. \tag{4.10}$$

For example, in a dynamo simulation with $\Lambda_o = 1$, $Pm = 1$, $Rm_o = 100$, we estimate that the value of the cross-over Ekman number will be of order 10^{-6}.

5. Discussion

The essential argument made here is that magnetostrophically balanced convection dynamics do not occur when the linear Elsasser number $\Lambda_o \sim 1$ as defined in (1.7), but rather when $\Lambda \sim 1$ as defined in (4.2). We estimate that this $\Lambda \sim 1$ transition is scale-dependent, and can be approximated to occur at the magnetostrophic cross-over flow scale $\ell_{\mathrm{X}} = \Lambda_o^2/Rm_o$. Thus, it is hypothesized that a magnetostrophically balanced convective state can exist only on scales below ℓ_{X} (figure 9). Because the system-scale value of Λ is typically less than unity in planetary dynamo models (table 1), our analysis implies that their large-scale convective flows must be in quasi-geostrophic balance [28,34,56]. Estimates suggest that $\ell_{\mathrm{X}} < 1$ for planets as well (table 2). Thus, large-scale quasi-geostrophic convective flows are hypothesized to exist in planetary core settings as well [26].

(a) Dynamo model implications

We hypothesize that local magnetostrophic convection dynamics can only exist in nonlinear dynamo systems on flow sclales below the magnetostrophic cross-over scale, $\ell_U \lesssim \ell_{\mathrm{X}}$. If this local magnetostrophic convection follows the linear predictions (figure 6), then we argue that the magnetostrophic convection scale will tend to increase, reaching up to a saturation value that lies in the vicinity of ℓ_{X}. If ℓ_U were to increase further still beyond ℓ_{X}, equation (4.7) implies that magnetostrophic conditions would no longer exist. Thus, if the saturation scales significantly exceeds ℓ_{X}, these flows will be quasi-geostrophic in nature, with magnetostrophic effects arising only at higher orders [26,66]. If the saturation scale were to significantly exceed ℓ_{X} [56], this would occur to due processes that are not likely to be magnetostrophic in nature, such as via a low Rossby number, high Reynolds number inverse hydrodynamic cascade (e.g. [67]).

It is reasonable that ℓ_χ could provide a magnetostrophic saturation scale in dynamo simulations (e.g. [20,28,34,56,63], cf. [68]). However, the value of ℓ_χ is probably not constant in these models. Because magnetic field strengths vary both spatially and temporally within dynamo generating regions, it is likely that the value of the cross-over scale will also vary with the local magnetic field intensity. This may explain, for example, the radially varying characteristic length scales found in figure 2 of Yadav *et al.* [27].

In rapidly rotating spheres and spherical shells, we put forward a more detailed prediction. In spherical systems, $\Lambda_o = 0$ rotating convection onsets with an $E^{1/3}D$ azimuthal scale [38,48]. Thus, the azimuthal wavenumber scales as $m \sim E^{-1/3}$. The axial length scale is system scale. The cylindrical scale is large as well, owing to the presence of broad spiral structures [48] or cylindrically radial sheets that can cross a significant portion of the fluid shell [69]. We hypothesize that it is only the azimuthal length scales that will tend to increase in scale to ℓ_χ in spherical dynamo systems. Thus, the azimuthal wavenumber will approach $m \sim \pi/\ell_\chi$ in regions of the fluid with $\Lambda \gtrsim 1$, as appears to be the case in the equatorial slices shown in Yadav *et al.*'s [34] figure 2 and in Aubert *et al.*'s [28] figure 5. It should be possible to test this hypothesis using spherical dynamo simulation results by making a scatter plot of the local azimuthal wavenumber m versus the local magnetic field intensity $B(\boldsymbol{x})$. Thus, from (4.6), we predict that the $m \sim E^{-1/3}$ rotating convection scaling trend will hold in regions where $\Lambda \lesssim 1$ and will transition to a local Elsasser number based scaling such that

$$m \propto \Omega^{1/3} \longrightarrow m \propto \frac{\Omega^2}{B(\boldsymbol{x})^4} \tag{5.1}$$

in magnetostrophic regions where $\Lambda \gtrsim 1$. We further argue that the magnetostrophic decrease in wavenumber ($m \propto B(\boldsymbol{x})^{-4}$) will create a feedback, driving the local value of Λ towards unity where the process will saturate.

Our cross-over scaling estimates lead us to argue that $\ell_\chi \gtrsim 1$ globally magnetostrophic dynamos are not likely to be accurate proxies for low ℓ_χ dynamo systems. Following Calkins *et al.* [26], we argue that the dynamical balance in $\Lambda \sim 1$, $\ell_\chi < 1$ regions will be locally magnetostrophic, but that the over-arching diagnostic force balance is still likely to remain geostrophic in nature. Evidence for this scenario exists in the study of Aubert *et al.* [28]. There they have generated a suite of $\Lambda_o \sim 20$, $Rm_o \sim 10^3$ spherical dynamo solutions using relatively low Pm, low E large-eddy simulations. In basic agreement with our ℓ_χ scaling estimates, spectral force plots (their figure 2) demonstrate that the solutions attain a zeroth-order, quasi-geostrophic diagnostic balance across scales, with first-order, magnetostrophic dynamical balance arising on smaller scales $\ell \lesssim 0.1$.

However, the cross-over scale's quadratic depence on Λ_o cannot be neglected in (4.7). For example, the $\ell_\chi \sim 1$ global magnetostrophic regime appears to have been reached in the spherical dynamo modelling study of Dormy [63]. Based on the results given in table 1 in [63], the 'strong field' cases have Λ_o exceeding 10 whilst $Rm_o \simeq 100$, such that $\ell_\chi \gtrsim 1$ and $\Lambda \gtrsim 1$. Because the cross-over scale appears to exceed the system scale in these $Pm \sim 10$ models, the convective flows may be in global (system-scale) magnetostrophic balance. Impressively, these models are found to display classically-predicted magnetostrophic dynamo behaviours, such as subcritical dynamo bifurcations [18].

(b) Planetary applications

Estimates of ℓ_χ are given in table 2 for all the dynamo-bearing planetary bodies in the solar system. Similar to our estimates for Earth, the planetary magnetostrophic cross-over scales all lie below the scales that are presently accessible to external observation [64,70]. The rightmost two columns in table 2 give the ratios of ℓ_χ with the turbulent $\Lambda_o = 0$ rotating convection scale, $\ell_{\text{turb}} \simeq Ro^{1/2}$, and the $\Lambda_o = 0$ rotating convection onset scale, $\ell_{\text{onset}} \simeq E^{1/3}$. The value of these length scale ratios provides an estimate of $\Lambda^{1/2}$ on that particular scale of flow. For example, if the $\ell_\chi/\ell_{\text{turb}} < 1$ for a given body, it is expected that motions occurring the turbulent scale of rotating

Table 2. Planetary estimates of magnetostrophic cross-over parameters. Planetary parameters values are estimated based on the values given in table 4 in [16]. However, their Λ_o estimates are multiplied by 10 to incorporate the effects of strong internal magnetic fields (cf. [4]).

	Λ_o	Rm_o	Pm	E	ℓ_χ	$\ell_\chi/\ell_{\text{turb}}$	$\ell_\chi/\ell_{\text{onset}}$
Mercury	10^{-4}	10^{2}	10^{-6}	10^{-12}	10^{-10}	10^{-8}	10^{-6}
Earth	10^{0}	10^{3}	10^{-6}	10^{-15}	10^{-3}	10^{0}	10^{2}
Eupiter	10^{1}	10^{3}	10^{-7}	10^{-19}	10^{-1}	10^{3}	10^{5}
Ganymede	10^{-2}	10^{2}	10^{-6}	10^{-13}	10^{-6}	10^{-4}	10^{-2}
Saturn	10^{-1}	10^{3}	10^{-7}	10^{-18}	10^{-5}	10^{-1}	10^{1}
Uranus	10^{-3}	10^{2}	10^{-8}	10^{-16}	10^{-8}	10^{-5}	10^{-3}
Neptune	10^{-3}	10^{2}	10^{-8}	10^{-16}	10^{-8}	10^{-5}	10^{-3}

convection will be largely unaffected by magnetic forces. If this length scale ratio is greater than unity, we predict that magnetostrophic effects can occur at that scale.

On Mercury, Ganymede, Uranus and Neptune, both length scale ratios are far less than one, implying that quasi-geostrophic convection exists in these bodies' cores from the system-scale all the way down the linear onset scale of rotating convection [26]. On Earth and Saturn, $\ell_\chi/\ell_{\text{onset}} \gtrsim 1$ and $\ell_\chi/\ell_{\text{turb}} \sim 1$, which suggests that magnetostrophic effects will exist at the smallest convection scales and may occur up to, but not far beyond, the $Ro^{1/2}$ turbulent scale. Finally, both length scale ratios are well above unity on Jupiter. Thus, magnetostrophic convection processes are expected to significantly alter the hydrodynamic convection scales there and may produce externally observable magnetostrophic signatures.

(c) Open questions and summary

Two fundamental simplifying assumptions have been made in developing our model for the magnetostrophic cross-over scale, which leave open paths to modify the cross-over scale for more complex systems. First, we have assumed in (4.4) that the magnetic induction processes are in quasi-static balance. This assumption is made based on the results of many present day, quasi-laminar (usually $Pm \sim 1$) dynamo models. In these models, the flows are nearly quasi-steady with local scale Reynolds numbers and magnetic Reynolds numbers close to unity. Thus, we argue that the local-scale induction will be well-described, at first order, by a quasi-static approximation [20,28,63]. However, it is not clear that quasi-steady induction accurately describes high Rm induction occurring on large scales in planetary settings where time variations may help balance the induction term [71,72]. Furthermore, as higher Reynolds number, lower Pm dynamo models are carried out, we expect that time varying inductive balances may become essential to include in cross-over scale models (cf. [56,68,73,74]).

Second, it is assumed, primarily for simplicity, that the velocity and magnetic magnitude estimates are scale invariant quantities each with well-defined variational scales. In fully turbulent magnetohydrodynamic settings, though, the velocity and magnetic fields are expected to be spectrally varying quantities [75,76]. If the magnetic and velocity fields have power law variations, then they can be expressed as

$$U \sim U_o \ell^{\alpha} \quad \text{and} \quad B \sim B_o \ell^{\beta}, \tag{5.2}$$

and (4.2) may be recast as

$$\Lambda = \left[\frac{\Lambda_o}{Rm_o}\right](\beta \ell^{(2\beta-\alpha-1)}). \tag{5.3}$$

The value of the Elsasser number in (5.3) can strongly depend on the values of the exponents, α and β, that describe the respective velocity and magnetic field spectra. Detailed predictions of α and β values are difficult to make with possible estimates easily ranging from $\alpha = 5$ to $\frac{5}{3}$ (e.g. figure 3b in [77]). However, what we can predict based on (5.3) is that qualitatively differing $\Lambda(\ell)$ behaviours should arise in the various regimes of multi-scale core flow, each likely having unique α and β values (e.g. figure 8 in [24]).

In sum, the results of our scaling arguments inspire great optimism for the future of planetary dynamo modelling. Many core dynamicists have surmised that because geodynamo models generate leading-order quasi-geostrophic flows, rather than magnetostrophic convective flows, they cannot be faithfully modelling core physics. In contrast, this work argues that $\Lambda_o \sim 1$ core convection should be quasi-geostrophically balanced on large scales $\ell \gtrsim \ell_\chi$, which are the only scales presently resolvable by geomagnetic field observations and by many numerical simulations of planetary dynamo action (figure 8*b*). At small scales below ℓ_χ, on the other hand, core dynamics may be well represented by rotating convection occurring in the presence of a strong magnetic field, not dissimilar from the conditions assumed by linear theory. Small-scale core flow may then be adequately modelled by turbulent rotating magnetoconvection studies [33,78]. Thus, in upcoming model generations, we must accurately incorporate the behaviour of the small-scale, magnetostrophic convective turbulence within a model of large-scale, quasi-geostrophic flow [26], which may then be compared reasonably with core flow inversions from geomagnetic secular variation observations [79].

Authors' contributions. J.A. and E.K. conceived of the core concepts and wrote the paper. J.A. produced the linear stability analysis, the dynamo model meta-analysis, and the figures. Both authors approve of this publication.
Competing interests. We declare we have no competing interests.
Funding. The support of the US National Science Foundation Geophysics Program (award no. 1547269) is gratefully acknowledged.
Acknowledgements. We thank M. Calkins for providing the linear stability solver used in making figures 2, 3, 5, 6 and 8, and for numerous discussions. Our further thanks to N. Schaeffer, A. Sheyko, K. Soderlund and B. Sreenivasan for providing the dynamo data in table 1 and for related discussions. The feedback from two constructive reviews also significantly improved our arguments.

References

1. Julien K, Rubio AM, Grooms I, Knobloch E. 2012 Statistical and physical balances in low Rossby number Rayleigh-Bénard convection. *Geophys. Astrophys. Fluid Dyn.* **106**, 392–428. (doi:10.1080/03091929.2012.696109)
2. Finlay C, Jackson A, Gillet N, Olsen N. 2012 Core surface magnetic field evolution 2000–2010. *Geophys. J. Int.* **189**, 761–781. (doi:10.1111/j.1365-246X.2012.05395.x)
3. Larson RL, Olson PL. 1991 Mantle plumes control magnetic reversal frequency. *Earth Planet. Sci. Lett.* **107**, 437–447. (doi:10.1016/0012-821X(91)90091-U)
4. Gillet N, Jault D, Canet E, Fournier A. 2010 Fast torsional waves and strong magnetic field within the Earth's core. *Nature* **465**, 74–77. (doi:10.1038/nature09010)
5. Finlay C, Olsen N, Kotsiaros S, Gillet N, Tøffner-Clausen L. 2016 Recent geomagnetic secular variation from Swarm and ground observatories as estimated in the CHAOS-6 geomagnetic field model. *Earth Planets Space* **68**, 112. (doi:10.1186/s40623-016-0486-1)
6. Chandrasekhar S. 1961 *Hydrodynamic and hydromagnetic stability*. Oxford, UK: Oxford University Press.
7. Buffett BA, Huppert HE, Lister JR, Woods AW. 1996 On the thermal evolution of the Earth's core. *J. Geophys. Res.* **101**, 7989–8006. (doi:10.1029/95JB03539)
8. Gubbins D. 2001 The Rayleigh number for convection in the Earth's core. *Phys. Earth Planet. Int.* **128**, 3–12. (doi:10.1016/S0031-9201(01)00273-4)
9. Le Bars M, Cébron D, Le Gal P. 2015 Flows driven by libration, precession, and tides. *Annu. Rev. Fluid Mech.* **47**, 163–193. (doi:10.1146/annurev-fluid-010814-014556)
10. O'Rourke J, Stevenson DJ. 2016 Powering Earth's dynamo with magnesium precipitation from the core. *Nature* **529**, 387–389. (doi:10.1038/nature16495)
11. Morgan J, Rupke LH, White WM. 2016 The current energetics of Earth's interior: A gravitational energy perspective. *Front. Earth Sci.* **4**, 13835. (doi:10.3389/feart.2016.00046)

12. Konopkova Z, McWilliams RS, Gomez-Perez N, Goncharov AF. 2016 Direct measurement of thermal conductivity in solid iron at planetary core conditions. *Nature* **534**, 99–101. (doi:10.1038/nature18009)
13. Ohta K, Kuwayama Y, Hirose K, Shimizu K, Ohishi Y. 2016 Experimental determination of the electrical resistivity of iron at Earth's core conditions. *Nature* **534**, 95–98. (doi:10.1038/nature17957)
14. Davies C, Pozzo M, Gubbins D, Alfé D. 2015 Constraints from material properties on the dynamics and evolution of Earth's core. *Nat. Geosci.* **8**, 678–685. (doi:10.1038/ngeo2492)
15. Roberts PH. 2007 Theory of the Geodynamo. In *Treatise on geophysics*, vol. 8. Amsterdam, The Netherlands: Elsevier.
16. Schubert G, Soderlund KM. 2011 Planetary magnetic fields: observations and models. *Phys. Earth Planet. Int.* **187**, 92–108. (doi:10.1016/j.pepi.2011.05.013)
17. Taylor JB. 1963 The magnetohydrodynamics of a rotating fluid and the Earth's dynamo problem. *Proc. R. Soc. Lond. A* **274**, 274–283. (doi:10.1098/rspa.1963.0130)
18. Roberts PH, King EM. 2013 On the genesis of the Earth's magnetism. *Rep. Prog. Phys.* **76**, 096801. (doi:10.1088/0034-4885/76/9/096801)
19. Cardin P, Brito D, Jault D, Nataf H-C, Masson J-P. 2002 Towards a rapidly rotating liquid sodium dynamo experiment. *Magnetohydrodynamics* **38**, 177–189.
20. Soderlund KM, King EM, Aurnou JM. 2012 The influence of magnetic fields in planetary dynamo models. *Earth Planet. Sci. Lett.* **333–334**, 9–20. (doi:10.1016/j.epsl.2012.03.038)
21. Jault D. 2008 Axial invariance of rapidly varying diffusionless motions in the Earth's core interior. *Phys. Earth Planet. Int.* **166**, 67–76. (doi:10.1016/j.pepi.2007.11.001)
22. Gillet N, Schaeffer N, Jault D. 2011 Rationale and geophysical evidence for quasi-geostrophic rapid dynamics within the Earth's outer core. *Phys. Earth Planet. Int.* **187**, 380–390. (doi:10.1016/j.pepi.2011.01.005)
23. Soderlund KM, Sheyko A, King EM, Aurnou JM. 2015 The competition between Lorentz and Coriolis forces in planetary dynamos. *Prog. Earth Planet. Sci.* **2**, 24. (doi:10.1186/s40645-015-0054-5)
24. Nataf H-C, Schaeffer N. 2015 Turbulence in the core. In *Treatise on geophysics*, 2nd edn., vol. 8. New York, NY: Elsevier.
25. Aubert J. 2015 Geomagnetic forecasts driven by thermal wind dynamics in the Earth's core. *Geophys. J. Int.* **203**, 1738–1751. (doi:10.1093/gji/ggv394)
26. Calkins MA, Julien K, Tobias S, Aurnou JM. 2015 A multiscale dynamo model driven by quasi-geostrophic convection. *J. Fluid Mech.* **780**, 143–166. (doi:10.1017/jfm.2015.464)
27. Yadav R, Gastine T, Christensen UR, Wolk SJ, Poppenhaeger K. 2016 Approaching a realistic force balance in geodynamo simulations. *Proc. Natl Acad. Sci. USA* **113**, 12 065–12 070. (doi:10.1073/pnas.1608998113)
28. Aubert J, Gastine T, Fournier A. 2017 Spherical convective dynamos in the rapidly rotating asymptotic regime. *J. Fluid Mech.* **813**, 558–593. (doi:10.1017/jfm.2016.789)
29. Gastine T, Wicht J, Aurnou JM. 2015 Turbulent Rayleigh--Bénard convection in spherical shells. *J. Fluid Mech.* **778**, 721–764. (doi:10.1017/jfm.2015.401)
30. Chandrasekhar S. 1954 The instability of a layer of fluid heated below and subject to the simultaneous action of a magnetic field and rotation. *Proc. R. Soc. Lond. A* **225**, 173–184. (doi:10.1098/rspa.1954.0195)
31. Eltayeb IA, Roberts PH. 1970 On the hydromagnetics of rotating fluids. *Astrophys. J.* **162**, 699–701. (doi:10.1086/150701)
32. Julien K, Knobloch E. 2007 Reduced models for fluid flows with strong constraints. *J. Math. Phys.* **48**, 065405. (doi:10.1063/1.2741042)
33. King EM, Aurnou JM. 2015 Magnetostrophic balance as the optimal state for turbulent magnetoconvection. *Proc. Natl Acad. Sci. USA* **112**, 990–994. (doi:10.1073/pnas.1417741112)
34. Yadav R, Gastine T, Christensen UR, Duarte LDV, Reiners A. 2016 Effect of shear and magnetic field on the heat-transfer efficiency of convection in rotating spherical shells. *Geophys. J. Int.* **204**, 1120–1133. (doi:10.1093/gji/ggv506)
35. Zhang K, Gubbins D. 2000 Is the geodynamo process intrinsically unstable? *Geophys. J. Int.* **140**, F1–F4. (doi:10.1046/j.1365-246x.2000.00024.x)
36. Eltayeb IA. 1972 Hydromagnetic convection in a rapidly rotating fluid layer. *Proc. R. Soc. Lond. A* **326**, 229–254. (doi:10.1098/rspa.1972.0007)
37. Eltayeb IA. 1975 Overstable hydromagnetic convection in a rotating fluid layer. *J. Fluid Mech.* **71**, 161–179. (doi:10.1017/S0022112075002480)

38. Zhang K, Schubert G. 2000 Magnetohydrodynamics in rapidly rotating spherical systems. *Annu. Rev. Fluid Mech.* **32**, 409–443. (doi:10.1146/annurev.fluid.32.1.409)
39. Sakuraba A. 2002 Linear magnetoconvection in rotating fluid spheres permeated by a uniform axial magnetic field. *Geophys. Astrophys. Fluid Dyn.* **96**, 291–318. (doi:10.1080/03091920290024234)
40. Cheng JS, Aurnou JM. 2016 Tests of diffusion-free scaling behaviors in numerical dynamo datasets. *Earth Planet. Sci. Lett.* **436**, 121–129. (doi:10.1016/j.epsl.2015.12.004)
41. Olson PL, Glatzmaier GA. 1995 Magnetoconvection in a rotating spherical shell: Structure of flow in the outer core. *Phys. Earth Planet. Int.* **92**, 109–118. (doi:10.1016/0031-9201(95)03065-5)
42. Fearn D. 1998 Hydromagnetic flow in planetary cores. *Rep. Prog. Phys.* **61**, 175–235. (doi:10.1088/0034-4885/61/3/001)
43. Cardin P, Olson P. 1995 The influence of toroidal magnetic field on thermal convection in the core. *Earth Planet. Sci. Lett.* **132**, 167–181. (doi:10.1016/0012-821X(95)00044-D)
44. King EM, Aurnou JM. 2013 Turbulent convection in liquid metal with and without rotation. *Proc. Natl Acad. Sci. USA* **110**, 6688–6693. (doi:10.1073/pnas.1217553110)
45. Julien K, Knobloch E. 1998 Strongly nonlinear convection cells in a rapidly rotating fluid layer: the tilted *f*-plane. *J. Fluid Mech.* **360**, 141–178. (doi:10.1017/S0022112097008446)
46. Zhang K, Gubbins D. 2000 Scale disparities and magnetohydrodynamics in the Earth's core. *Phil. Trans. R. Soc. Lond. A* **358**, 899–920. (doi:10.1098/rsta.2000.0566)
47. Calkins MA, Aurnou JM, Eldredge JD, Julien K. 2012 The influence of fluid properties on the morphology of core turbulence and the geomagnetic field. *Earth Planet. Sci. Lett.* **359–360**, 55–60. (doi:10.1016/j.epsl.2012.10.009)
48. Dormy E, Soward AM, Jones CA, Jault D, Cardin P. 2004 The onset of thermal convection in rotating spherical shells. *J. Fluid Mech.* **501**, 43–70. (doi:10.1017/S0022112003007316)
49. Calkins MA, Julien K, Marti P. 2013 Three-dimensional quasi-geostrophic convection in the rotating cylindrical annulus with steeply sloping endwalls. *J. Fluid Mech.* **732**, 214–244. (doi:10.1017/jfm.2013.309)
50. Glatzmaier GA. 2002 Geodynamo simulations - how realistic are they? *Annu. Rev. Earth Planet. Sci.* **30**, 237–257. (doi:10.1146/annurev.earth.30.091201.140817)
51. King EM, Buffett BA. 2013 Flow speeds and length scales in geodynamo models: the role of viscosity. *Earth Planet. Sci. Lett.* **371–372**, 156–162. (doi:10.1016/j.epsl.2013.04.001)
52. Aurnou JM, Calkins MA, Cheng JS, Julien K, King EM, Nieves D, Soderlund KM, Stellmach S. 2015 Rotating convective turbulence in Earth and planetary cores. *Phys. Earth Planet. Int.* **246**, 52–71. (doi:10.1016/j.pepi.2015.07.001)
53. Sreenivasan B. 2010 Modelling the geodynamo: progress and challenges. *Curr. Sci.* **99**, 1739–1749.
54. Soderlund KM, King EM, Aurnou JM. 2014 Corrigendum to 'The influence of magnetic fields in planetary dynamo models'. *Earth Planet. Sci. Lett.* **392**, 121–123. (doi:10.1016/j.epsl.2014.01.052)
55. Sheyko A. 2014 Numerical investigations of rotating MHD in a spherical shell. Ph.D. thesis. Zurich, Switzerland: ETH.
56. Schaeffer N, Jault D, Nataf H-C, Fournier A. Submitted. Geodynamo simulations with vigorous convection and low viscosity. *Geophys. J. Int.* (https://arxiv.org/abs/1701.01299v1)
57. Christensen UR, Aubert J. 2006 Scaling properties of convection-driven dynamos in rotating spherical shells and application to planetary magnetic fields. *Geophys. J. Int.* **00**, 97–114. (doi:10.1111/j.1365-246X.2006.03009.x)
58. Gastine T, Wicht J, Aubert J. 2016 Scaling regimes in spherical shell rotating convection. *J. Fluid Mech.* **808**, 690–732. (doi:10.1017/jfm.2016.659)
59. Jones CA, Soward AM, Mussa AI. 2000 The onset of thermal convection in a rapidly rotating sphere. *J. Fluid Mech.* **405**, 157–179. (doi:10.1017/S0022112099007235)
60. Roberts PH. 1968 On the thermal instability of a rotating-fluid sphere containing heat sources. *Phil. Trans. R. Soc. Lond. A* **263**, 93–117. (doi:10.1098/rsta.1968.0007)
61. Busse FH. 1970 Thermal instabilities in rapidly rotating systems. *J. Fluid Mech.* **44**, 441–460. (doi:10.1017/S0022112070001921)
62. Aubert J, Brito D, Nataf H-C, Cardin P, Masson J-P. 2001 A systematic experimental study of rapidly rotating spherical convection in water and liquid gallium. *Phys. Earth Planet. Int.* **128**, 51–74. (doi:10.1016/S0031-9201(01)00277-1)
63. Dormy E. 2016 Strong-field spherical dynamos. *J. Fluid Mech.* **789**, 500–513. (doi:10.1017/jfm.2015.747)

64. Ridley VA, Holme R. 2016 Modeling the Jovian magnetic field and its secular variation using all available magnetic field observations. *J. Geophys. Res. Planets* **121**, 309–337. (doi:10.1002/2015JE004951)
65. Schaeffer N, Pais MA. 2011 On symmetry and anisotropy of Earth-core flows. *Geophys. Res. Lett.* **38**, L10309. (doi:10.1029/2011GL046888)
66. Sreenivasan B, Sahoo S, Dhama G. 2014 The role of buoyancy in polarity reversals of the geodynamo. *Geophys. J. Int.* **199**, 1698–1708. (doi:10.1093/gji/ggu340)
67. Rubio A, Julien K, Knobloch E, Weiss JB. 2014 Upscale energy transfer in three-dimensional rapidly rotating turbulent convection. *Phys. Rev. Lett.* **112**, 144501. (doi:10.1103/PhysRevLett.112.144501)
68. Sheyko A, Finlay CC, Jackson A. 2016 Magnetic reversals from planetary dynamo waves. *Nature* **539**, 551–554. (doi:10.1038/nature19842)
69. Sumita I, Olson P. 2000 Laboratory experiments on high rayleigh number thermal convection in a rapidly rotating hemispherical shell. *Phys. Earth Planet. Int.* **117**, 153–170. (doi:10.1016/S0031-9201(99)00094-1)
70. Anderson BJ *et al.* 2011 The global magnetic field of Mercury from MESSENGER orbital observations. *Science* **333**, 1859–1862. (doi:10.1126/science.1211001)
71. Finlay CC, Dumberry M, Chulliat A, Pais MA. 2010 Short timescale core dynamics: theory and observations. *Space Sci. Rev.* **155**, 177–218. (doi:10.1007/s11214-010-9691-6)
72. Livermore P, Hollerbach R, Finlay CC. 2016 An accelerating high-latitude jet in Earth's core. *Nat. Geosci.* **10**, 62–68. (doi:10.1038/ngeo2859)
73. Dietrich W, Schmitt D, Wicht J. 2013 Hemispherical parker waves driven by thermal shear in planetary dynamos. *Eur. Phys. Lett.* **104**, 49001. (doi:10.1209/0295-5075/104/49001)
74. Hori K, Jones CA, Teed RJ. 2015 Slow magnetic rossby waves in the Earth's core. *Geophys. Res. Lett.* **42**, 6622–6629. (doi:10.1002/2015GL064733)
75. Kinney RM, McWilliams JC. 1998 Turbulent cascades in anisotropic magnetohydrodyna-mics. *Phys. Rev. E* **57**, 7111–7121. (doi:10.1103/PhysRevE.57.7111)
76. Christensen UR, Olson PL, Glatzmaier GA. 1999 Numerical modelling of the geodynamo: A systematic parameter study. *Geophys. J. Int.* **138**, 393–409. (doi:10.1046/j.1365-246X.1999.00886.x)
77. Cabanes S, Aurnou JM, Favier B, Le Bars M. In press. A laboratory model for deep-seated jets on the gas giants. *Nat. Phys.* (doi:10.1038/nphys4001)
78. Matsushima M, Nakajima T, Roberts PH. 1999 The anisotropy of local turbulence in the Earth's core. *Earth Planets Space* **51**, 277–286. (doi:10.1186/BF03352231)
79. Gillet N, Pais MA, Jault D. 2009 Ensemble inversion of time-dependent core flow models. *Geochem. Geophys. Geosyst.* **10**, Q06004. (doi:10.1029/2008GC002290)